

Amorphous silicon-doped titania films for on-chip photonics

Thomas Kornher,^{1,*} Kangwei Xia,¹ Roman Kolesov,¹ Bruno Villa,² Stefan Lasse,¹ Cosmin S. Sandu,³ Estelle Wagner,³ Scott Harada,³ Giacomo Benvenuti,³ Hans-Werner Becker,⁴ and Jörg Wrachtrup¹

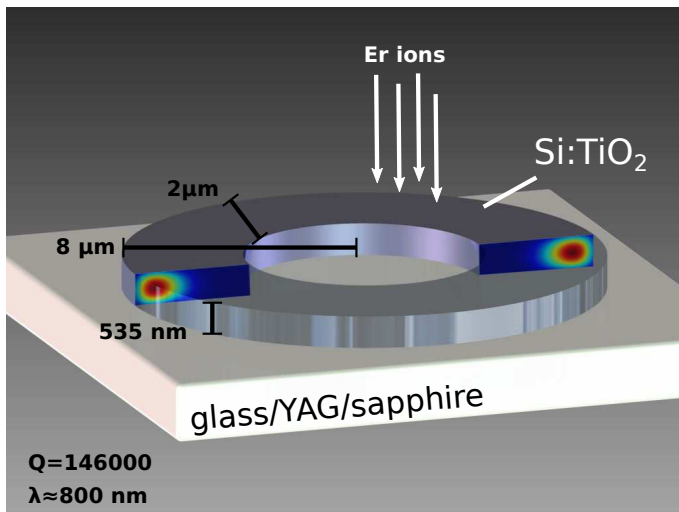
¹*Physikalisches Institut, Universität Stuttgart, 70569 Stuttgart, Germany*

²*Semiconductor Physics Group, Cavendish Laboratory, JJ Thomson Avenue, Cambridge, CB3 0HE, UK*

³*3D-OXIDES, 130 Rue Gustave Eiffel, Saint Genis Pouilly, 01630, France*

⁴*RUBION, Ruhr-Universität Bochum, 44780 Bochum, Germany*

High quality optical thin film materials form a basis for on-chip photonic micro- and nano-devices, where several photonic elements form an optical circuit. Their realization generally requires the thin film to have a higher refractive index than the substrate material. Here, we demonstrate a method of depositing amorphous 25% Si doped TiO₂ films on various substrates, a way of shaping these films into photonic elements, such as optical waveguides and resonators, and finally, the performance of these elements. The quality of the film is estimated by measuring thin film cavity Q-factors in excess of 10⁵ at a wavelength of 790 nm, corresponding to low propagation losses of 5.1 db/cm. The fabricated photonic structures were used to optically address chromium ions embedded in the substrate by evanescent coupling, therefore enabling it through film-substrate interaction. Additional functionalization of the films by doping with optically active rare-earth ions such as erbium is also demonstrated. Thus, Si:TiO₂ films allow for creation of high quality photonic elements, both passive and active and also provide access to a broad range of substrates and emitters embedded therein.



Introduction

Nanoscale fabrication of optical waveguide structures offers a wide range of opportunities spanning from on-chip photonic devices for optical networks to sensor applications. At the heart of such devices commonly lies a certain functionality that can be readily interfaced with other components, and be included into sophisticated architectures as it is standard with silicon-on-chip technology [1]. Material systems hardly compatible with silicon photonics, such as YAG, YSO or sapphire crystals, can host a large variety of emitters with applications ranging from quantum communication [2–4] and quantum memories [5, 6] to lasing materials [7, 8]. To exploit their potential in a scalable architecture, these substrates need to be

enabled by a waveguiding platform. Previously demonstrated photonic structures in these materials based on femtosecond laser-writing share common drawbacks like a low refractive index contrast between waveguide and substrate [9]. The corresponding increase of the minimum feature size of photonic elements by up to two orders of magnitude makes this technology unpractical for the field of cavity quantum electrodynamics (CQED) and nanoscale photonics in general.

An alternative way to realize a waveguiding platform is the deposition of a high refractive index thin film on top of these substrate crystals, which then provides on-chip access to these systems through evanescent light fields [10, 11] coupling to embedded emitters. Moreover, this approach leaves the substrate crystal untouched from processing and preserves the spectroscopic properties of embedded emitters [12].

In the visible range, titanium dioxide (TiO₂) features the highest refractive index out of a variety of transparent thin film materials, thus allowing for waveguiding on the majority of transparent substrates. Additionally, it has a wide transparency range covering the whole visible and near-infrared spectral regions. Shaping the deposited TiO₂ film into photonic elements can then be conveniently done by reactive ion etching (RIE) [13]. The deposited TiO₂ films often tend to form nano-crystallites which lead to significant scattering and, therefore, to substantial optical losses [14, 15]. The best performance is typically shown by amorphous TiO₂ films featuring a refractive index between 2.3 and 2.4 [15–19]. In order to preserve the amorphous composition of the film, special precautions have to be taken.

In the present work, we report on Chemical Beam Vapour Deposition (CBVD) of high optical quality Si:TiO₂ film whose amorphous state is preserved by doping with silicon [20]. The amorphisation of deposited TiO₂ with Si

* t.kornher@physik.uni-stuttgart.de

doping was already reported [21], and a more recent detailed study of amorphisation of Nb:TiO₂ thin films by doping with Si is reported elsewhere [22]. Even though this doping leads to a slight decrease in the refractive index of the film, in agreement with results achieved with other Chemical Vapour deposition techniques [23], the index is still high enough to support waveguiding on high-index optical crystals such as YAG and sapphire. On the other hand, Si doping keeps the TiO₂ from forming nanocrystallites even at elevated temperatures up to 650°C, resolving the inherent thermal instability of amorphous TiO₂ films to some extent [24].

The optical performance of the film was assessed by fabricating whispering gallery mode (WGM) cavities and measuring their Q-factor. The latter was in excess of 10⁵. Evanescent coupling to fluorescent spots in the substrate material can be shown and also additional functionality can be added to the Si:TiO₂ film by doping it with fluorescent rare-earth ions, such as erbium. This shows the potential of Si:TiO₂ nanophotonic structures to also act as active elements within photonic devices.

Deposition of Si:TiO₂ combinatorial film

Oxide thin films were deposited by CBVD, as described in detail elsewhere [21]. The CBVD process makes use of thermal decomposition of organometallic precursors on a heated substrate in a high vacuum environment ($\leq 10^{-3}$ Pa). These precursors impinge upon the substrate as molecular beams and do not undergo any gas phase reaction. Deposition was conducted on epi-polished YAG crystals (CrysTec) and quartz for functional characterization and on Si and glass wafers for material characterization. The liquid organometallic precursors used during the present investigation were titanium tetraisopropoxide (Ti(OiPr)₄, CAS 546-68-9) evaporated from a reservoir at 32°C and tetrabutoxysilane (Si(OnBu)₄, CAS 4766-57-8, evaporated from a reservoir at 65°C). The Ti and Si precursor flows were homogeneously distributed on the substrate (the flow ratio of precursors was estimated as Si/Ti=1.1). The substrate temperature during the deposition was kept at 500°C. Under these conditions, the Si doping in the film (defined as Si/(Si+Ti) ratio) was about 25% (as measured by SEM-EDX) and the growth rate was about 10 ± 2 nm/min. Before starting the deposition, the chamber was pumped to a base pressure of 5×10^{-4} Pa. A liquid nitrogen-cooled cryo-panel helped to maintain a pressure below 2×10^{-3} Pa during the deposition. The morphology and the chemical composition of the thin films were investigated by SEM-EDX using a Merlin SEM and in TEM cross-section using a Tecnai Osiris microscope. From cross-sectional TEM images, we can estimate the average thickness of deposited films and their growth morphology. Typical images of characterized films are presented in Figure 1 a) and b) for films of thicknesses 800 ± 100 nm. A High Angle Annular Dark Field image (Figure 1 a) shows a homogeneous compact

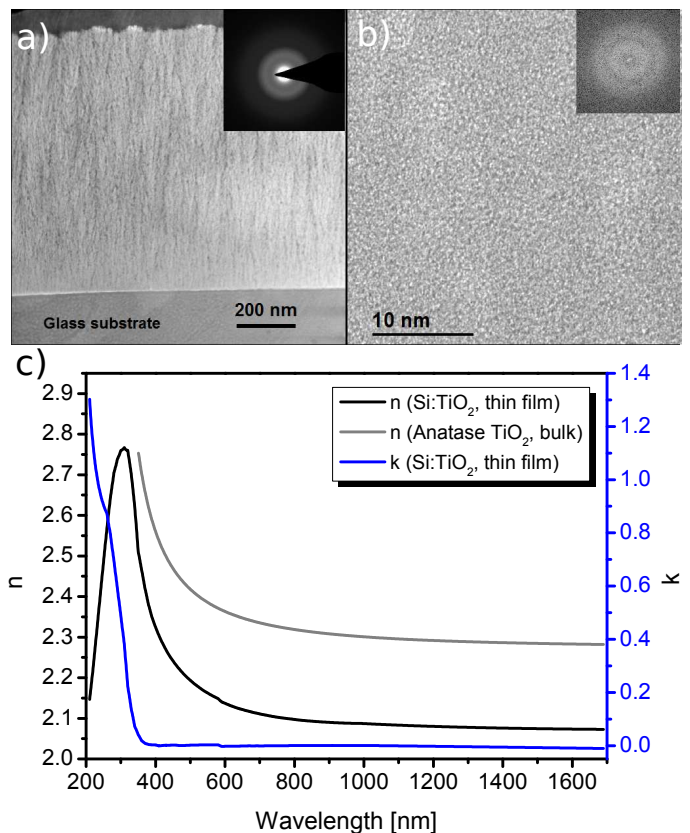


FIG. 1. Cross-sectional view by TEM of a Si:TiO₂ film deposited on glass substrate. a) HAADF-STEM image and SAED pattern. b) HRTEM image with inserted FFT. c) Refractive index for an unpatterned Si:TiO₂ film on silica sample and for comparison the refractive index of bulk anatase TiO₂ [25]. n and k denote the refractive index and the extinction coefficient, respectively.

film with relatively low roughness. The inserted Selected Area Electron Diffraction pattern together with the High Resolution TEM image (Figure 1 b) confirm the amorphous phase of the film. Further characterization of the unpatterned Si:TiO₂ film of a thickness of 535 nm by ellipsometry yields the dispersion of the refractive index as shown in figure 1 c). Within the transparency window of the film starting roughly at 400 nm and extending all the way to the infrared, the refractive index ranges between 2.3 and 2.1.

Structuring Si:TiO₂ films

In order to assess the optical quality of the film, we fabricated monolithic optical WGM resonators and tested the width of their resonances. The resonators were microrings evanescently coupled to a nearby optical waveguide through which excitation light was supplied.

The patterning was done by standard RIE with a Ni mask defined by e-beam lithography. RIE of Si:TiO₂ was performed in an atmosphere of Ar/CF₄/O₂ with the respective flow rates 4/16/3 sccm and the RF power

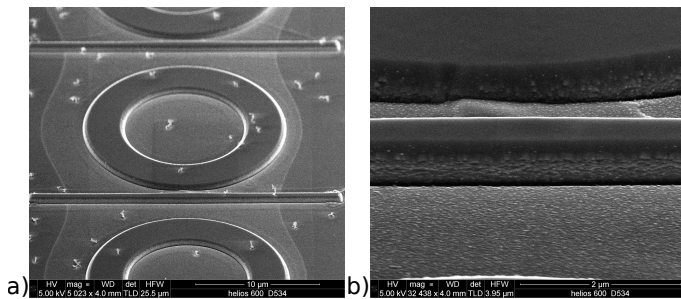


FIG. 2. a) SEM image of a Si:TiO₂ WGM resonator evanescently coupled to a straight optical waveguide. b) Close-up of the coupling region between ring resonator and access waveguide.

being 100 W [26]. The process pressure was 15 mTorr and the total time required to etch through 535 nm of Si:TiO₂ was 24 minutes. After etching, the nickel mask was still present indicating that the etching selectivity was better than 1:11. The residual nickel mask was removed by dissolving the metal in an aqueous 1M solution of nitric acid. In order to remove damage introduced into Si:TiO₂ films by ion bombardment during plasma etching, the resulting structures were annealed in air for 4 hours at 500°C. However, annealing the film at temperatures above 800°C leads to a visual change of the film, suggesting recrystallization. Sample SEM images of the resulting structures are shown in Figure 2. The radius of the WGM resonator was 8 μm while the length of the waveguide was 25 μm. The distance between the resonator and the waveguide was around 400 nm.

Optical characterization of waveguides and resonators on various substrates

In the following, waveguides and resonators were fabricated out of Si:TiO₂ thin films on two different substrates, namely YAG and silica with a refractive index of 1.82 and 1.45 at 790 nm, respectively. Studies of the optical performance of waveguides and cavities were performed in a home-built confocal microscope with an additional ability of scanning the detection point in the vicinity of the position of the excitation laser focus [27]. Its schematic is shown in Figure 3 a). The excitation laser was focused onto the sample with a high numerical aperture objective lens (Olympus 0.95×50).

A YAG crystal (Y₃Al₅O₁₂) was doped with chromium by ion implantation through a perforated copper mask with an average hole diameter of ≈400 nm. With an energy of 100 keV and a dose of 10¹² cm⁻², Cr ions end up in the YAG crystal in a depth of ≈ 56 ± 22 nm according to SRIM simulations [28]. A Si:TiO₂ film was subsequently deposited and shaped into waveguides in order to assess waveguiding and evanescent coupling of waveguided light to shallow implanted Cr-doped spots. Cr fluorescence of implanted spots could be detected close to 700 nm un-

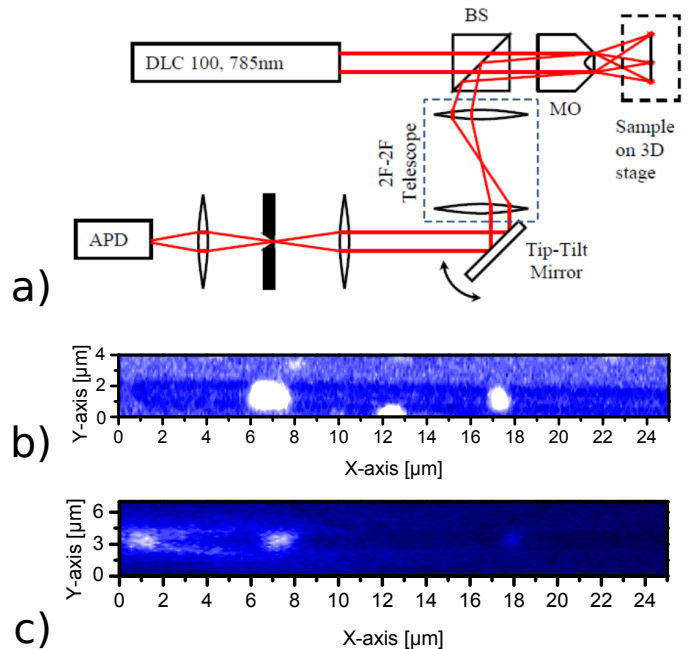


FIG. 3. a) Schematic diagram of the microscope. The sample is mounted on the 3D nanopositioner and can be moved through the laser focus. Light emission is collected through the same objective lens and sent through a 2F-2F telescope and a tip-tilt mirror onto the pinhole selecting the observation point on the sample. b) Standard confocal microscope scan with overlapping excitation and observation point. White spots represent fluorescence of Cr implanted spots in YAG, two of them underneath a fabricated Si:TiO₂ waveguide. c) Tip-tilt mirror scan with excitation point kept at a stationary position to couple light into the fabricated Si:TiO₂ waveguide (left end). The two white spots at around 7 μm and 18 μm on the X-axis represent fluorescence of Cr implanted spots, evanescently excited by light traveling through the waveguide.

der excitation with 600 nm light as shown in the confocal scan in Figure 3 b). Since the refractive index of YAG is smaller than the index of the film, waveguiding could be observed. Incoupled light traveling within the waveguide was able to evanescently excite Cr implanted spots as shown in the tilting mirror scan in Figure 3 c). Here, the excitation laser position was kept stationary coupling light into the left end of the waveguide. By scanning the point of detection with the tilting mirror, not only the excitation laser position yields signal, but also implanted Cr spots light up, which are embedded below the waveguide extending to the right. This confirms the evanescent coupling of light between fabricated waveguide and emitters in the substrate. In combination with high quality resonators, this film-substrate interaction has the potential to facilitate CQED experiments with rare-earth ion doped crystals [12].

For characterizing fabricated Si:TiO₂ resonators on glass substrates, the widths of the cavity resonances were studied with a single frequency tunable diode laser (Top-

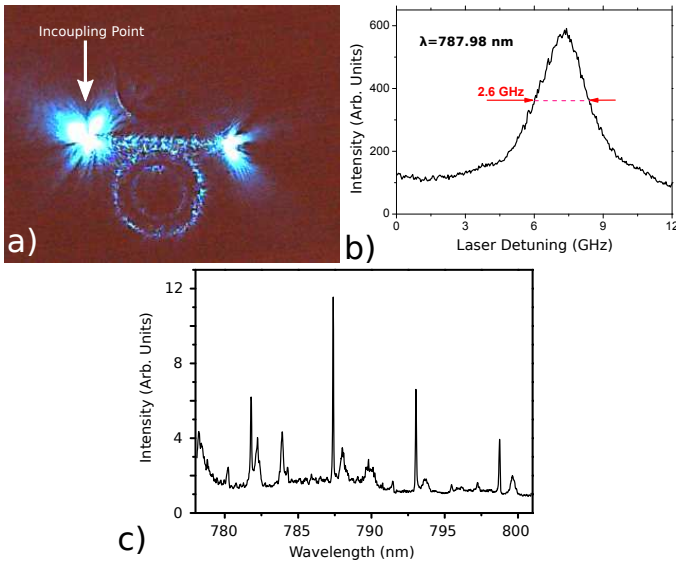


FIG. 4. a) Camera image of a structure excited on resonance. The left end of the waveguide was used as input and the cavity mode is visualized by the residual scattering of the laser being in resonance. Tunable blue diode laser was used for visualization. b) The spectral shape of the cavity mode was obtained by sweeping a single-mode laser through the cavity resonance. c) Typical mode spectrum of the studied resonator geometry between 780 nm and 800 nm obtained with a broadband light source. Mode width measurement is limited by the resolution of the spectrometer for the fundamental mode.

tica DL Pro). The laser could be tuned coarsely over the range of 770-800 nm with a mode-hop-free fine tuning range of 30 GHz. The spectral width of the laser was below 1 MHz. Laser output was inserted into one of the ends of the optical waveguide and its frequency was swept while monitoring the scattered emission at the rim of the cavity. The rim lit up once the laser was in resonance with one of the cavity modes due to residual scattering on the imperfections of the structured film (see Figure 4 a)). This scattering was detected as a function of laser frequency to estimate the spectral width of the mode. The result of the spectral measurements is shown in Figure 4 b). The estimated mode width was 2.6 GHz as the laser was finely swept around 787.89 nm wavelength. This value corresponds to the quality factor of $Q \approx 146000$. For this specific resonator geometry with an outer resonator radius of $R = 8 \mu\text{m}$, a film thickness of 535 nm and a rim width of $2 \mu\text{m}$, the mode spectrum was measured with a broadband light source in a wavelength region between 780 nm and 800 nm in order to extract the free spectral range (FSR) of $\Delta\lambda_{\text{FSR}} = 5.60 \text{ nm}$ for the fundamental mode. Including the refractive index measurement, our corresponding finite element method based simulation can confirm the measured FSR for the fundamental mode in this resonator geometry. The respective resonator sketch and the electric field profile of the mode is shown in Figure 5. With the FSR measurement around 790 nm, the group index of 2.18 was estimated

by $n_g \approx \lambda^2 / (2\pi R \cdot \Delta\lambda_{\text{FSR}})$. Based on the quality factor measurement and the group index estimation, propagation losses α in fabricated waveguides of 5.1 dB/cm were estimated by $\alpha = 2\pi n_g / Q\lambda$.

Table I compares different TiO_2 -based thin film waveguiding structures based on their propagation loss. The doped Si: TiO_2 film reaches benchmark propagation losses in the visible in exchange for a doping dependent decrease of the refractive index.

TABLE I. Comparison of propagation loss in dB/cm in TiO_2 -based thin film waveguiding structures.

Film details	Loss at 600-800 nm	Loss at 1550 nm	Reference
RF magnetron sputtering	9	4	[17]
laser molecular beam epitaxy	57	-	[14]
atomic layer deposition	-	2.4	[16]
RF magnetron sputtering	9.7	-	[19]
CBVD	5.1	-	this work

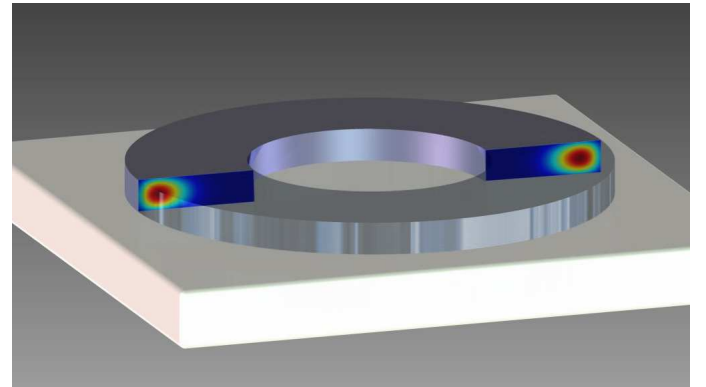


FIG. 5. Resonator sketch with calculated electric field profile of the fundamental 790-nm mode.

Doping of Si: TiO_2 resonators with erbium

Another way of adding functionality to the thin film, specifically to the fabricated thin film resonators, is by optical activation with fluorescent species. We have chosen rare-earth (RE) doping due to robust optical properties of RE ions in most crystalline and glassy transparent media. RE doping can be performed by ion implantation with very high yield of fluorescent species [29]. In addition, optical materials doped with erbium exhibit strong upconverted fluorescence in the visible once excited in the infrared. This makes erbium doping conveniently detectable. The Si: TiO_2 film on glass was implanted with erbium ions of 2 MeV energy and with a dose of 10^{14} cm^{-2} . According to SRIM simulations, this

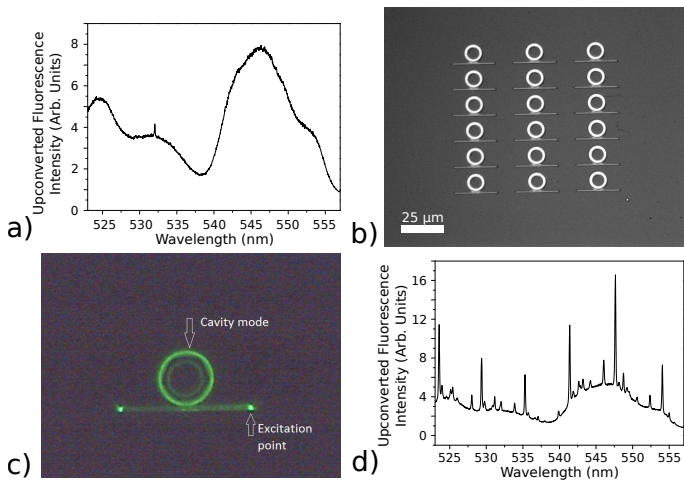


FIG. 6. a) Spectrum of upconverted fluorescence of erbium in Si:TiO₂ film. Excitation wavelength is 785 nm. b) Microscope image of the WGM resonators manufactured out of Er³⁺-implanted film. Scale bar is 25 μm long. c) Cavity mode visualized by upconverted fluorescence. The excitation laser is in resonance with one of the infrared cavity modes. d) Spectrum of erbium upconverted fluorescence collected at the end of the waveguide. The smooth background is due to the fluorescence of the waveguide. The sharp peaks correspond to resonances of the cavity.

leads to an erbium doping inside the Si:TiO₂ film in a depth of $\approx 350 \pm 78$ nm, corresponding to a maximum local density of $5 \cdot 10^{18} \text{ cm}^{-3}$ [28]. Immediately after the implantation, the appearance of the film was changed from pink to grey, probably, due to implantation-induced damage. At this point no upconverted fluorescence from Er³⁺ ions was detected. Post-implantation annealing in air at 500°C for 4 hour heals out the implantation damage and, at the same time, activates erbium emission. After annealing, the film restored its original color. At the same time, strong green upconverted fluorescence of erbium ions could be detected under the excitation with red (650 nm) and infrared (800 nm) laser light. The spectrum of the upconverted emission is shown in Figure 6 a), in good agreement with other works on erbium in glassy environment [30, 31].

The film was shaped to form whispering gallery mode cavities with 5 μm radius coupled to straight waveguides as described above (see Figure 6 b). The upconversion resonances of Er³⁺ in glassy environment are broad (≈ 10 nm), therefore, several infrared cavity modes could lead to upconverted fluorescence. Once the infrared excitation laser is tuned in resonance with one of such modes, green fluorescence on the rim of the WGM cavity lights up (see Figure 6 c, the excitation laser is filtered out). The spectrum of the fluorescence collected at one of the waveguide ends shows its mode structure as indicated in Figure 6 d).

Conclusion

We have demonstrated a method of depositing low loss high index Si:TiO₂ films on different substrates such as glass, sapphire, and YAG. For most substrates, the refractive index of the film is high enough to support waveguiding and also evanescently excite shallow fluorescent centers within the substrate material. We have also shown a way of structuring the film to form on-chip photonic elements such as waveguides and resonators. The low propagation loss of 5.1 dB/cm results in a high Q-factor of the resonators (1.5×10^5 at 800 nm) and underlines the potential for CQED application in connection with rare-earth ion doped crystals for example. Finally, due to the increased thermal stability of this film when compared to TiO₂, we could demonstrate further optical functionalization of the film by doping with fluorescent rare-earth species (erbium). These results show how the silicon doped titania film can be applied to on-chip photonics in various ways.

Acknowledgements

The authors wish to thank the CIME-EPFL team for their TEM investigation facilities. The authors wish to acknowledge the FEDER (Fonds Européen de Développement Economique et Régional) for financing the Nanobium project through the Interreg IVA programme. The work was also financed by ERC SQUITEC, EU-SIQS SFB TR21, and DFG KO4999/1-1.

-
- [1] J. Hulme, J. Doylend, M. Heck, J. Peters, M. Davenport, J. Bovington, L. Coldren, and J. Bowers, *Opt. Express* **23**, 5861 (2015).
 - [2] R. Kolesov, K. Xia, R. Reuter, R. Stöhr, A. Zappe, J. Meijer, P. Hemmer, and J. Wrachtrup, *Nat. Commun.* **3**, 1029 (2012).
 - [3] T. Utikal, E. Eichhammer, L. Petersen, A. Renn, S. Gtzinger, and V. Sandoghdar, *Nat. Commun.* **5**, 3627 (2014).
 - [4] R. Kolesov, K. Xia, R. Reuter, M. Jamali, R. Stöhr, T. Inal, P. Siyushev, and J. Wrachtrup, *Phys. Rev. Lett.* **111**, 120502 (2013).
 - [5] M. Zhong, M. P. Hedges, R. L. Ahlefeldt, J. G. Bartholomew, S. E. Beavan, S. M. Wittig, J. J. Longdell, and M. J. Sellars, *Nature* **517**, 177 (2015).
 - [6] C. Clausen, I. Usmani, F. Bussi eres, N. Sangouard, M. Afzelius, H. de Riedmatten, and N. Gisin, *Nature* **469**, 508 (2011).
 - [7] P. Moulton, *Optics News* **8**, 9 (1982).
 - [8] T. H. Maiman, *Nature* **187**, 493 (1960).
 - [9] T. Calmano, J. Siebenmorgen, O. Hellmig, K. Petermann, and G. Huber, *Appl. Phys. B* **100**, 131 (2010).
 - [10] E. Vetsch, D. Reitz, G. Sagu e, R. Schmidt, S. Dawkins, and A. Rauschenbeutel, *Phys. Rev. Lett.* **104**, 203603 (2010).

- (2010).
- [11] L. Liebermeister, F. Petersen, A. v. Münchow, D. Burhardt, J. Hermelbracht, T. Tashima, A. W. Schell, O. Benson, T. Meinhardt, A. Krueger, A. Stiebeiner, A. Rauschenbeutel, H. Weinfurter, and M. Weber, *Appl. Phys. Lett.* **104**, 031101 (2014).
- [12] S. Marzban, J. G. Bartholomew, S. Madden, K. Vu, and M. J. Sellars, *Phys. Rev. Lett.* **115**, 013601 (2015).
- [13] R. Quidant, J.-C. Weeber, A. Dereux, G. Lévêque, J. Weiner, and C. Girard, *Phys. Rev. B* **69**, 081402 (2004).
- [14] K. Abe, E. Y. M. Teraoka, T. Kita, and H. Yamada, *Proc. SPIE*, 79401 (2011).
- [15] T. Alasaarela, L. Karvonen, H. Jussila, A. Säynätjoki, S. Mehravar, R. A. Norwood, N. Peyghambarian, K. Kieu, I. Tittonen, and H. Lipsanen, *Opt. Lett.* **38**, 3980 (2013).
- [16] M. Häyrinen, M. Roussey, V. Gandhi, P. Stenberg, A. Säynätjoki, L. Karvonen, M. Kuittinen, and S. Honkanen, *J. Lightwave Technol.* **32**, 208 (2014).
- [17] J. D. Bradley, C. C. Evans, J. T. Choy, O. Reshef, P. B. Deotare, F. Parsy, K. C. Phillips, M. Lončar, and E. Mazur, *Opt. Express* **20**, 23821 (2012).
- [18] J. T. Choy, J. D. Bradley, P. B. Deotare, I. B. Burgess, C. C. Evans, E. Mazur, and M. Lončar, *Opt. Lett.* **37**, 539 (2012).
- [19] M. Furuhashi, M. Fujiwara, T. Ohshiro, M. Tsutsui, K. Matsubara, M. Taniguchi, S. Takeuchi, and T. Kawai, *AIP Adv.* **1**, 032102 (2011).
- [20] P. Karasiński, C. Tyszkiewicz, R. Rogoziński, J. Jaglarz, and J. Mazur, *Thin Solid Films* **519**, 5544 (2011).
- [21] E. Wagner, C. S. Sandu, S. Harada, C. Pellodi, M. Jobin, P. Mural, and G. Benvenuti, *ACS Comb. Sci.* **18**, 154 (2016).
- [22] C. Sandu, E. Wagner, S. Harada, G. Benvenuti, W. Maudez, M. Jobin, C. Pellodi, and P. Mural, *Thin Solid Films* **615**, 265 (2016).
- [23] S.-M. Lee, J.-H. Park, K.-S. Hong, W.-J. Cho, and D.-L. Kim, *J. Vac. Sci. Technol., A* **18**, 2384 (2000).
- [24] N. Martin, C. Rouselot, D. Rondot, F. Palmino, and R. Mercier, *Thin solid films* **300**, 113 (1997).
- [25] J. R. DeVore, *J. Opt. Soc. Am.* **41**, 416 (1951).
- [26] K.-R. Choi, J.-C. Woo, Y.-H. Joo, Y.-S. Chun, and C.-I. Kim, *Vacuum* **92**, 85 (2013).
- [27] R. Kolesov, B. Grotz, G. Balasubramanian, R. J. Stöhr, A. A. Nicolet, P. R. Hemmer, F. Jelezko, and J. Wrachtrup, *Nat. Phys.* **5**, 470 (2009).
- [28] J. F. Ziegler, M. D. Ziegler, and J. P. Biersack, *Nucl. Instrum. Methods Phys. Res., Sect. B* **268**, 1818 (2010).
- [29] T. Kornher, K. Xia, R. Kolesov, N. Kukharchyk, R. Reuter, P. Siyushev, R. Stöhr, M. Schreck, H.-W. Becker, B. Villa, A. D. Wieck, and J. Wrachtrup, *Appl. Phys. Lett.* **108**, 053108 (2016).
- [30] F. Vetrone, J.-C. Boyer, J. A. Capobianco, A. Speghini, and M. Bettinelli, *Appl. Phys. Lett.* **80**, 1752 (2002).
- [31] F. Song, G. Zhang, M. Shang, H. Tan, J. Yang, and F. Meng, *Appl. Phys. Lett.* **79**, 1748 (2001).